Research Square

Preprints are preliminary reports that have not undergone peer review.
They should not be considered conclusive, used to inform clinical practice,
or referenced by the media as validated information.

Integrative bioinformatics prioritises exosome-associated Epstein- Barr virus microRNA targets in gastric cancer

Megha Chandran
Chosun University
Seung Rim Hwang
srhwang@chosun.ac.kr
Chosun University

Research Article

Keywords: Epstein–Barr virus (EBV), Gastric cancer, Exosomal miRNA, BamHI-A rightward transcript (BART), CLASH, Toll-like receptor (TLR) signalling

Posted Date: October 5th, 2026

DOI: https://doi.org/10.21203/rs.3.rs-10795593/v1

License: This work is licensed under a Creative Commons Attribution 4.0 International License. Read Full License

Additional Declarations: No competing interests reported.

Abstract

Background

Epstein-Barr virus (EBV)-associated gastric cancer (EBVaGC) is characterised by substantial immune-cell infiltration and frequent amplification or overexpression of programmed death (PD)-ligand 1 and PD-ligand 2. Nevertheless, the molecular mechanisms that may contribute to immune regulation in this cancer subtype remain incompletely understood. EBV-positive SNU719 gastric cancer cells produce BamHI-A rightward transcript (BART) microRNAs (miRNAs), some of which are packaged into exosomes while also remaining detectable in the parental cells. This study aimed to identify EBV BART miRNAs relatively enriched in SNU719-derived exosomes and to investigate their candidate interactions with human transcripts involved in innate immune signalling.

Results

Publicly available datasets were integrated through a CLASH-guided multilayer computational framework. Parental-cell and exosomal miRNA profiles were compared to identify exosome-enriched EBV BART miRNAs. SNU719-specific CLASH data were then used to identify reproducible viral miRNA interactions with human transcripts in the toll-like receptor (TLR)/nuclear factor kappa-light-chain-enhancer of activated B cells/interferon regulatory factor pathway. Network topology and perturbation analyses ranked the most influential miRNA candidates, while SNU719 RNA-seq data confirmed expression of most prioritised human target transcripts. This integrated analysis identified 11 reproducible miRNA-target interactions and prioritised BART17-5p, BART8-3p, and BART10-3p as the strongest candidate exosome-associated EBV BART miRNAs. The Cancer Genome Atlas-Stomach Adenocarcinoma analysis did not reveal significant EBV-status-dependent differences in bulk TLR-related pathway scores.

Conclusions

The study provides a reusable computational framework for prioritizing exosome-associated viral miRNA-human target interactions from public multi-omic datasets. BART17-5p, BART8-3p, and BART10-3p emerged as experimentally testable candidates linked to innate immune signalling in EBVaGC.

Background

Gastric cancer remains a major global health burden, with approximately 1.1 million new cases and 770,000 deaths estimated worldwide in 2020 [1]. Epstein–Barr virus (EBV)-associated gastric cancer (EBVaGC) represents a distinct molecular subtype and accounts for approximately 8–10% of gastric adenocarcinomas worldwide. The Cancer Genome Atlas (TCGA) classified EBVaGC as one of the four principal molecular subtypes of gastric cancer and identified characteristic alterations, including recurrent PIK3CA mutations, extensive DNA hypermethylation, and amplification of the 9p24.1 region containing Janus kinase 2, CD274, and PDCD1LG2, which encode programmed death (PD)-ligand 1 and PD-ligand 2, respectively [2]. EBVaGC also commonly exhibits substantial lymphocytic infiltration and increased immune-checkpoint ligand expression, indicating an immunologically active tumour microenvironment. Nevertheless, this immune-active phenotype does not consistently result in effective antitumour immunity, suggesting that additional viral and cellular regulatory mechanisms may contribute to immune escape in this disease subtype.

Extracellular vesicles (EVs) provide a potential route through which EBV-positive tumour cells may influence surrounding cells. These membrane-bound particles transport proteins, lipids, messenger RNAs (mRNAs), microRNAs (miRNAs), and other biologically active molecules between cells [3, 4]. Small EVs commonly described as exosomes arise through the endosomal pathway and can protect their RNA cargo from extracellular degradation. In cancer, tumour-derived exosomes can modify immune cell activation, differentiation, and intercellular communication. The minimal information for studies of EVs 2018 (MISEV2018) guidelines emphasize the need for careful terminology and cautious functional interpretation, particularly when vesicle identity and biological activity have not been fully established.

EBV can exploit EV-mediated communication to deliver viral regulatory molecules to uninfected recipient cells. Mature EBV-encoded miRNAs released from infected B cells have been detected in exosomes and transferred to monocyte-derived dendritic cells, where they regulate immunologically relevant targets such as C-X-C motif chemokine 11 [5]. This observation demonstrated that EBV miRNAs can act beyond the infected cell through vesicle-mediated transfer. Similar forms of EV communication have also been reported in EBV-associated epithelial malignancies. Exosomes derived from EBV-positive nasopharyngeal carcinoma cells have been shown to contain viral and host regulatory molecules capable of altering signalling responses in recipient cells [6]. These findings support the possibility that EV cargo contributes to communication between EBV-positive tumour cells and the surrounding microenvironment.

EBV encodes numerous mature miRNAs, most of which originate from the BamHI-A rightward transcript region and are collectively known as BamHI-A rightward transcript (BART) miRNAs. These miRNAs are highly expressed during latent EBV infection in epithelial malignancies and can regulate human gene expression through Argonaute-mediated binding to target RNAs. BART miRNAs have been associated with viral persistence, cellular survival, and immune-evasion processes. Their biological relevance is difficult to determine through sequence-based target prediction alone, as computational methods often generate large numbers of potential targets. Experimental evidence of miRNA-target binding is therefore important for identifying interactions that occur within living cells.

Cross-linking, ligation, and sequencing of hybrids (CLASH) can provide direct biochemical evidence of miRNA-target RNA association. The method captures Argonaute-associated miRNAs together with the RNA fragments to which they are bound and sequences the resulting chimeric molecules. Ungerleider and colleagues used CLASH to map EBV miRNA-human RNA interactions in the naturally EBV-positive SNU719 gastric cancer cell line and the Akata lymphoma cell line [7]. This dataset provided an experimentally grounded view of EBV miRNA targeting. The original analysis was not designed to determine which interacting EBV miRNAs were relatively enriched in exosomes, nor did it specifically prioritise interactions involving toll-like receptor (TLR), nuclear factor kappa-light-chain-enhancer of activated B cells (NF-κB), and interferon regulatory factor signalling. CLASH therefore can provide evidence of intracellular miRNA-RNA binding, while functional repression and activity in recipient cells require separate experimental confirmation.

The SNU719 cell line provides a relevant model for connecting these evidence layers, as it is a naturally EBV-infected gastric cancer cell line that maintains a latent viral-expression programme representative of EBV-associated gastric epithelial malignancy [8, 9]. Publicly available small-RNA sequencing data from SNU719 parental cells and SNU719-derived exosomal preparations allow the identification of EBV BART miRNAs that are relatively enriched in the exosomal fraction [8]. These miRNAs are not necessarily exclusive to exosomes. Their relative abundance is greater in the exosomal fraction than in the corresponding parental cells. Combining these data with

SNU719-specific CLASH interactions and SNU719 transcriptomic profiles creates an opportunity to link exosomal enrichment with experimentally observed human RNA targets and cellular expression context.

TLR signalling was selected as the principal biological pathway for this analysis due to its central role in antiviral and inflammatory responses. Nucleic-acid-sensing TLRs recognise viral RNA or DNA within endosomal compartments and transmit signals through adaptor proteins and kinases, including myeloid differentiation primary response 88 (MYD88), TIR domain containing adaptor molecule 1, interleukin-1 receptor associated kinase (IRAK)-family proteins, tumour necrosis factor receptor-associated factor, and TANK-binding kinase 1 (TBK1). These signalling cascades activate NF-κB components and interferon regulatory factor (IRF) such as IRF3 and IRF7, leading to inflammatory cytokine production and type I interferon responses [9, 10]. EBV BART miRNAs that bind human RNA transcripts encoding components of these pathways may represent candidate regulators of innate immune signalling. Such regulatory effects cannot be concluded from binding evidence alone and require functional validation.

A pathway-restricted list of miRNA-target pairs may overlook the broader regulatory structure of viral miRNAs. Individual EBV miRNAs can bind multiple human transcripts, and their direct targets may connect indirectly to pathway outputs through protein-protein interaction networks. Network analysis can therefore complement pathway filtering by identifying miRNAs that occupy influential positions within integrated miRNA-target and protein-interaction structures. Centrality measures and in silico perturbation analyses can estimate whether removal of a particular viral miRNA substantially alters network connectivity. These analyses provide a systematic basis for prioritisation, while remaining computational indicators rather than evidence of confirmed biological regulation.

This study addresses three linked gaps. First, no previous analysis has connected EBV BART miRNAs relatively enriched in SNU719-derived exosomes with CLASH-supported human transcript targets in the TLR/NF-κB/IRF pathway. Second, existing EBV miRNA studies have not integrated gastric cancer-specific CLASH interactions with exosomal enrichment and cellular target-expression data. Third, no transparent computational workflow has combined these evidence layers with network topology and tumour-cohort contextualisation in EBVaGC.

We therefore developed a CLASH-guided multilayer evidence framework to identify and prioritise exosome-associated EBV BART miRNA-human transcript interactions linked to innate immune signalling. The framework integrates parental-cell and exosomal miRNA profiles, reproducible SNU719 CLASH interactions, pathway-aware filtering, heterogeneous miRNA-target-protein interaction networks, perturbation-based hub ranking, SNU719 RNA-seq expression support, and TCGA-Stomach Adenocarcinoma (STAD) contextualisation. The objective was not to demonstrate immune suppression, tumour development, or tumour progression. Instead, the study aimed to generate a ranked and evidence-tiered set of candidate miRNA-target interactions for future reporter assays, miRNA perturbation studies, and exosome-recipient-cell experiments. The workflow was designed as a modular and reusable computational strategy that may be applied to other virus-associated cancers and EV miRNA datasets.

Table 1
Comparison of closely related published studies.

Study	Model	Data type	Approach	TLR pathway	Exosomal context	Gap addressed here
Ungerleider et al. 2021 [11]	SNU719, Akata	CLASH miRNA-seq	EBV miRNA targetome mapping	Immune enrichment noted, but TLR genes not specifically filtered	Not examined	We filter SNU719 CLASH interactions for TLR genes and link them to exosomal cargo
Lin et al. 2023 [8]	SNU719 cells and exosomes	Small RNA-seq	EBV miRNA cargo profiling	Not examined	Exosome miRNA profiling performed	We integrate their cargo data with CLASH and network analysis
TCGA Research Network 2014 [12]	295 gastric adenocarcinomas	Multi-omics	Molecular subtyping	Not examined	Not examined	We use TCGA-STAD for clinical contextualization of SNU719 predictions

The five-step computational workflow starts with SNU719 exosomal miRNA cargo profiling, filters SNU719-specific CLASH interactions against curated TLR/NF-κB/IRF pathway genes, prioritises candidate miRNAs using multilayer network perturbation, applies SNU719 RNA-seq expression support, and finally evaluates whether the resulting pathway signature is reflected in TCGA-STAD bulk-tumour data. To our knowledge, this is the first CLASH-guided exosomal miRNA evidence-integration framework that links EBV BART miRNA cargo, experimentally observed host interactions, TLR/NF-κB/IRF pathway architecture, network perturbation, and tumour-cohort contextualisation in EBV-associated gastric cancer. The workflow is illustrated in Fig. 1.

[Figure 1 here]

Figure 1. **Overview of the CLASH-guided multilayer evidence framework used to prioritise exosomal EBV BART miRNA-host interactions in EBV-associated gastric cancer.**

Public datasets were integrated across five analytical modules. 1)SNU719 exosomal miRNA-seq data from GSE227017 were analysed using edgeR TMM normalisation and differential enrichment analysis to identify significantly and moderately enriched EBV miRNAs. 2) SNU719-specific CLASH interactions from GSE147228 were filtered for interactions present across three biological replicates and intersected with a curated 38-gene TLR/NF-κB/IRF innate immune pathway set. 3) pathway mapping identified 11 reproducible EBV miRNA-to-TLR-pathway interactions involving seven pathway genes. 4) CLASH miRNA-mRNA edges were integrated with STRING protein-protein interaction data to construct a heterogeneous network and perform topology and perturbation analyses, prioritising BART17-5p as the dominant hub. 5) SNU719 RNA-seq data from GSE239994 provided transcriptomic support for expressed miRNA-target pairs, while TCGA-STAD and GSE62254 were used for tumour-context contextualisation and workflow portability assessment. The integrated output prioritised BART17-5p, BART8-3p, and BART10-3p as experimentally testable exosomal EBV BART miRNA candidates linked to innate immune signalling, without implying functional validation.

Methods

Data Source and Accession Numbers

All data used in this study are publicly available from the Gene Expression Omnibus (GEO) and NCI Genomic Data Commons (GDC). No new human data were generated, and institutional review board approval was not required. The dataset sources and their analytical roles are summarised in Table 2.

The GSE227017 dataset was generated by Lin et al. and contains miRNA expression profiles for three replicates each of SNU719 cells, SNU719-derived exosomes, AGS cells (human gastric adenocarcinoma cells), and AGS-derived exosomes [8]. Exosome characterisation, including nanoparticle tracking analysis, transmission electron microscopy, and CD63/CD81 western blotting, was performed as described in a previous study [8]. The GSE147228 CLASH dataset was generated by Ungerleider et al. and includes three biological replicates of CLASH in SNU719 and Akata cells [7]. Protein–protein interaction data for network construction were obtained from the STRING database version 11.5 for *Homo sapiens* at a minimum combined confidence score of 0.4, downloaded programmatically at runtime using the STRINGdb R package. Only the SNU719 CLASH files were used in the main analysis. The GSE239994 RNA-seq dataset provides whole-transcriptome RNA-seq data for SNU719 cells across three biological replicates [13]. TCGA-STAD RNA-seq, miRNA-seq, and clinical data were accessed using the GDC Data Portal. GSE62254 was used as an independent gastric context cohort [14].

- Exosomal miRNA enrichment analysis

Raw count columns from the GSE227017 files were extracted from all 12 samples. The files contained three columns: miRNA_ID, Total_Count, and Normalised _Value. Total_Count values were used as input for differential expression analysis, as normalised _Value had already been processed and could distort the library size estimation. EBV miRNA entries were retained, and miRNAs with fewer than 0.5 counts per million in at least two samples were excluded, leaving 43 testable miRNAs.

Normalisation was performed using edgeR trimmed mean of M-values (TMM) normalization [15]. Differential enrichment between SNU719 exosomes and SNU719 parent cells was tested using the edgeR quasi-likelihood F-test. Group A was defined as statistically enriched miRNAs with false discovery rate (FDR)-adjusted p-value < 0.05 and log2 fold change > 1. Group B was defined as a secondary moderately enriched group with a log2 fold change > 0.8 and an FDR between 0.05 and 0.15. Group C showed significantly depleted miRNA levels. Visualisation was performed using ggplot2 and pheatmap. Principal component analysis was performed on the TMM-normalised log2CPM values using prcomp in R.

- CLASH parsing and TLR-pathway filtering

Only the SNU719 CLASH files from GSE147228 were used: GSM4421234, GSM4421235, and GSM4421236. The Akata files were excluded to maintain the focus on gastric cancer. Each CLASH file contained two columns: a combined miRNA Target Gene identifier and an interaction score. Interactions were parsed by splitting the combined identifiers into a single underscore delimiter. Interaction scores were aggregated across replicates by calculating the mean score, and replicate counts were used to track reproducibility. Only interactions present in all three SNU719 replicates were used as high-confidence pairs.

A curated 38-gene TLR pathway set was compiled from the KEGG Toll-like receptor signalling pathway hsa04620 and published TLR signalling reviews [9]. The gene set included sensors, adaptors, kinases, transcription factors, NF-κB components, cytokines, and interferon-response genes. A complete curated gene list is provided in

Supplementary Table S2. CLASH interactions were cross-referenced against this gene set to identify EBV miRNA-TLR pathway interactions.

Pathway enrichment analysis was performed using clusterProfiler [16] on all 11,808 unique host gene targets from SNU719 EBV CLASH interactions. KEGG gene IDs were obtained using org.Hs.eg.db annotations. The multiMiR package was used to query the experimentally validated and predicted targets using miRTarBase, TargetScan, and miRDB. Given the incomplete representation of EBV BART miRNAs in human miRNA target databases, CLASH was used as the primary source of evidence for interaction.

- Network construction and topology analysis

A heterogeneous network was constructed using igraph in R [17]. Layer 1 connects the exosomal EBV BART miRNAs from Groups A and B to their SNU719 CLASH-supported host gene targets. Layer 2 connected host target genes to TLR pathway components through STRING protein–protein interactions downloaded using STRINGdb with humans as the species and a minimum confidence score of 0.4. Edge weights were assigned using CLASH, meaning interaction scores for miRNA-target edges, and STRING combined scores for protein-protein interaction (PPI) edges.

- Sensitivity analysis

To evaluate the robustness of the network prioritisation, the perturbation analysis was repeated using a higher STRING confidence threshold of 0.7. Candidate miRNA rankings were compared across the default and high-confidence networks using betweenness centrality, node strength, and percentage reduction in weighted TLR reachability.

Network topology metrics included degree centrality, betweenness centrality, and node strength. Community detection uses Louvain modularity optimisation. In silico knockdown was performed by removing each EBV miRNA node individually and recalculating weighted TLR reachability. Weighted reachability was defined as the sum of the edge weights of the paths from the remaining miRNA nodes to TLR pathway nodes. The percentage reduction in reachability after the removal of each miRNA was used as the perturbation score. Focused subnetworks were generated for the TLR7/8 and TLR9/type I interferon modules by retaining the top bridge genes with STRING PPI connections to the core pathway nodes. Network figures were generated using igraph and ggraph [17, 18].

- SNU719 transcriptomic expression filtering

SNU719 RNA-seq count data from GSE239994 were loaded as a matrix of 57,736 Ensembl gene IDs across three replicates [13]. Ensembl IDs were mapped to HGNC gene symbols using org.Hs.eg.db. After deduplication, 34,728 unique gene symbols were identified. Curated TLR pathway genes were extracted from the mapped matrices. Expression classes were defined as high, mean count ≥ 100; expressed, 10 to 99 counts; low, 1 to 9 counts; and not detected, 0 counts.

For directional miRNA-target concordance analysis, EBV BART miRNA counts from SNU719 small-RNA sequencing companion files in GSE147228 were used as miRNA-side data and the mean CPM values from GSE239994 RNA-seq were used as mRNA-side data. As these data came from separate GEO series rather than from matched samples, concordance was interpreted descriptively rather than as formal statistical evidence. The EBV latency context was inferred from the BART:BHRF1 expression ratio using small RNA counts following published latency interpretation criteria [7].

- TCGA-STAD bulk-tumour contextualisation

The GDC file UUIDs were mapped to TCGA patient barcodes by querying the GDC API file endpoint using the manifest file IDs as filters. The EBV-positive status was assigned by cross-referencing TCGA patient barcodes against a curated list of 25 known EBV-positive TCGA-STAD cases derived from the TCGA-STAD 2014 supplementary data and published curations [2]. Cases that were not on the EBV-positive list were designated as EBV negative.

The TCGA miRNA-seq files were loaded using reads_per_million_miRNAs_mapped as a normalised expression measure. The TCGA RNA-seq files were loaded using an unstranded count column in an augmented STAR count format. The TLR pathway activity was scored using single-sample GSEA with GSVA [19]. Six gene sets were scored: TLR signalling, TLR sensors, TLR adaptors, NF-κB, IFN response, and cytokines. EBV-positive versus EBV-negative comparisons were performed using the Wilcoxon rank-sum test with Benjamini–Hochberg FDR correction.

Immune cell deconvolution was performed using the immunedeconv R package, with an MCP-counter [20]. Survival analysis was performed using the survival R package [21] and survminer for visualisation. Overall survival time was derived from days_to_death and days_to_last_follow_up, with vital_status used as the event indicator. Kaplan–Meier curves were estimated using survival routines and compared using the log-rank test. Cox proportional hazards regression included TLR_signalling score, IFN response score, EBV status, and AJCC pathological stage as covariates.

Statistical analysis

Differential expression analyses were performed using Benjamini–Hochberg FDR correction. Group comparisons were performed using Wilcoxon rank-sum tests. Survival curves were compared using log-rank tests. The Cox model assumptions were evaluated using the Schoenfeld residuals. Analyses were performed using R version 4.5 with Bioconductor version 3.20. The package versions are provided in the final code repository. The analysis scripts, processed results tables, and plotting codes were deposited in a public repository before publication. A private review link will be provided upon submission if available.

- Reproducibility and code organisation

All analyses were implemented as scripted R workflows organised into five modules: exosomal miRNA enrichment, CLASH pathway filtering, network construction and perturbation, SNU719 transcriptomic expression filtering, and TCGA-STAD contextualisation. Intermediate processed tables and plotting scripts were saved to allow regeneration of all main and supplementary figures. The code, processed result tables, and figure-generation scripts are available in this repository https://github.com/MeghaChandran06/ebvagc-exosomal-bart-tlr-network .

Table 2
Modular workflow structure and analytical outputs.

Workflow module	Input data	Main output	Related figure/table
Exosomal miRNA enrichment	GSE227017	Group A/B/C EBV miRNA candidates	Figure 2, Table 3
CLASH pathway filtering	GSE147228	11 reproducible TLR-pathway interactions	Figure 3, Table 4
Network perturbation	CLASH + STRING	Hub-ranked exosomal EBV miRNAs	Figure 4, Table 5
Expression filtering	GSE239994	Expression-confirmed miRNA-target pairs	Figure 5, Table 6
Tumour contextualisation	TCGA-STAD and GSE62254	Bulk pathway context and boundary analysis	Figure 6, Table 7

Results

- SNU719 exosomes contain a restricted set of enriched EBV BART miRNAs

AGS samples carried near-zero EBV miRNA counts, ranging between 53–103 reads per sample, confirming the expected EBV negative control pattern. SNU719 cell libraries ranged from 2.5 million to 4.3 million reads mapping to EBV miRNAs, whereas SNU719 exosome libraries ranged from 443,000 to 1.9 million reads. These library size differences indicated that exosomal EBV miRNA profiles should be interpreted after normalisation rather than by raw abundance alone. TMM-normalised differential enrichment analysis supported non-random partitioning of specific EBV miRNAs between cells and exosomes.

Principal component analysis of all 12 samples confirmed the global separation between EBV-positive SNU719 and EBV-negative AGS samples. PC1 explained 43.2% of the variance and distinguished EBV-positive from EBV-negative samples, whereas PC2 explained 15.4% of the variance and captured partial variation between SNU719 cells and exosomes. Since PCA mainly serves as a quality control step, it is shown in Supplementary Figure S1.

Differential enrichment analysis between SNU719 exosomes and SNU719 cells identified three Group A miRNAs with FDR < 0.05 and log2FC > 1: ebv-miR-BART1-5p, ebv-miR-BART2-3p, and ebv-miR-BHRF1-2-3p. Four additional miRNAs, ebv-miR-BART13-5p, ebv-miR-BART17-5p, ebv-miR-BART10-3p, and ebv-miR-BART8-3p, formed a moderately enriched group. Four miRNAs were significantly depleted in the exosomes and retained in the cells, including ebv-miR-BART17-3p. The opposing behaviours of BART17-5p and BART17-3p are consistent with selective miRNA partitioning into exosomes rather than a simple proportional export of the cellular miRNA pool (Fig. 2).

[Figure 2 here]

Figure 2. **Differential EBV miRNA enrichment in SNU719 exosomes.**

Alt text: Volcano plot comparing EBV miRNA enrichment between SNU719 exosomes and SNU719 cells. Red points indicate miRNAs enriched in exosomes, blue points indicate miRNAs depleted from exosomes, and grey points

indicate non-significant miRNAs. BART1-5p, BART2-3p, and BHRF1-2-3p are enriched in exosomes, while BART17-3p and other miRNAs are depleted.

Table 3 summarises the exosome-enriched EBV miRNAs. Although BHRF1-2-3p was statistically enriched, it had very low abundance and was annotated as lytic-associated; therefore, it was not treated as a core latent BART candidate in the downstream TLR analysis. BART1-5p was the strongest exosomal hit, based on its abundance and fold enrichment. BART10-3p, BART17-5p, and BART8-3p did not meet the strict FDR threshold; nevertheless, they were retained as moderately enriched candidates owing to their abundance and subsequent CLASH and network support.

Table 3
EBV BART miRNAs enriched in SNU719 exosomes (Group A and Group B).

miRNA	Cell mean CPM	Exosome mean CPM	Enrichment ratio	log2FC	FDR	Group
ebv-miR-BART1-5p	164,825	565,691	3.43x	1.779	0.0051	A
ebv-miR-BART2-3p	273	1,031	3.77x	1.918	0.0314	A
ebv-miR-BHRF1-2-3p	6.7	52.9	7.74x	3.260	0.0314	A (lytic)
ebv-miR-BART13-5p	462	1,166	2.52x	1.336	0.053	B
ebv-miR-BART17-5p	1,215	2,992	2.46x	1.300	0.124	B
ebv-miR-BART10-3p	9,453	19,387	2.05x	1.036	0.098	B
ebv-miR-BART8-3p	1,502	2,796	1.86x	0.893	0.098	B

The full exosomal EBV miRNA abundance ranking is provided in Supplementary Figure S3. A heatmap of the top 20 EBV miRNAs confirmed broad separation of SNU719 and AGS samples and is provided as Supplementary Figure S2. Together, these results established a restricted exosomal EBV miRNA candidate set for downstream CLASH filtering.

- SNU719-only CLASH filtering identifies reproducible EBV miRNA interactions with TLR/NF-κB/IRF genes

Parsing of the three SNU719 CLASH replicates yielded 476,625 EBV miRNA interactions mapped to 40 unique EBV miRNAs and 11,808 unique host gene targets. Cross-referencing these interactions against the curated 38-gene TLR pathway set identified 74 EBV miRNAs involved in TLR-pathway interactions. Among these, 11 interactions involved the moderately exosome-enriched Group B miRNAs BART17-5p, BART8-3p, and BART10-3p and were present across all three biological replicates. No strict Group A miRNAs showed a reproducible direct CLASH interaction with the curated TLR pathway gene set.

This three-of-three replicate reproducibility provides strong biochemical support for recurrent Ago-associated miRNA target binding within the CLASH framework, although it does not prove target repression by itself. The alluvial mapping showed that the strongest cumulative CLASH signal flowed toward TF/NF-κB and kinase modules. Both BART8-3p and BART17-5p target NFKB1 and NFKB2, whereas BART17-5p and BART10-3p converge on IRAK1. BART8-3p and BART10-3p target IRF3. This pattern suggests coordinated candidate regulation of multiple levels of TLR/NF-κB/IRF signalling (Fig. 3).

[Figure 3 here]

Figure 3. **Reproducible Epstein–Barr virus (EBV) microRNA (miRNA) interactions using Toll-like receptor (TLR)-pathway genes**.

Alt text: Alluvial plot showing reproducible EBV miRNA interactions with TLR pathway genes based on SNU719 CLASH data. BART17-5p, BART8-3p, and BART10-3p connect to TLR-related targets including NFKB1, NFKB2, IRAK1, IRF3, TAB2, TIRAP, RELA, and IKBKG, with flows grouped into adaptor, kinase, regulatory, and TF/NF-κB functional modules.

Table 4 presents 11 high-confidence interactions. BART17-5p had the broadest direct TLR pathway-targeting profile, with six CLASH-supported interactions: NFKB2, TAB2, IRAK1, IKBKG, TIRAP, and RELA. BART8-3p carried the highest individual interaction score through NFKB1. BART10-3p contributes to the convergent targeting of IRAK1 and IRF3.

Table 4
High-confidence EBV exosomal miRNA to TLR pathway CLASH interactions (all present in 3 of 3 replicates).

miRNA	TLR target	Module	Mean CLASH score	Max CLASH score	Enrichment group
ebv-miR-BART8-3p	NFKB1	TF/NF-κB	10.53	26.31	B
ebv-miR-BART17-5p	NFKB2	TF/NF-κB	9.57	25.07	B
ebv-miR-BART8-3p	NFKB2	TF/NF-κB	4.77	9.02	B
ebv-miR-BART17-5p	Table 2	Kinase	3.11	7.33	B
ebv-miR-BART17-5p	IRAK1	Kinase	3.11	7.33	B
ebv-miR-BART10-3p	IRAK1	Kinase	3.11	7.33	B
ebv-miR-BART17-5p	IKBKG	Kinase	2.10	4.29	B
ebv-miR-BART10-3p	IRF3	Regulatory	1.55	2.65	B
ebv-miR-BART8-3p	IRF3	Regulatory	1.55	2.65	B
ebv-miR-BART17-5p	TIRAP	Adaptor	1.55	2.65	B
ebv-miR-BART17-5p	RELA	TF/NF-κB	1.55	2.65	B

Untargeted KEGG enrichment of all SNU719 EBV miRNA CLASH targets revealed broad enrichment for viral infections, endocytosis, transcriptional regulation, and immune-related pathways. TLR signalling did not emerge as a significant global term, supporting the use of targeted TLR pathway filtering rather than relying on global enrichment alone. This analysis is presented in Supplementary Figure S5.

A heatmap of CLASH interaction scores further showed that BART8-3p and BART17-5p had the strongest TLR pathway interaction scores among the exosome-associated miRNAs, particularly NFKB1 and NFKB2 (Supplementary Figure S4).

- Network perturbation prioritises BART17-5p, BART8-3p, and BART10-3p

The heterogeneous network contained 5,292 nodes and 16,027 edges, integrating 7,979 CLASH miRNA-target edges with 8,048 STRING protein–protein interaction edges. Of these nodes, 37 corresponded to TLR pathway components and 982 nodes had at least one weighted regulatory path to the TLR pathway. The baseline-weighted reachability score across the EBV miRNA-to-TLR pathways was 11,679.81.

Given the visual density of the full network, the complete network is provided as Supplementary Figure S6. In the main text, the network influence is summarised using topology and in silico perturbation metrics. BART17-5p was ranked first by betweenness centrality and produced the largest reduction in modelled TLR reachability after individual node removal. BART8-3p and BART10-3p were ranked second and third, respectively. BART1-5p was the most abundant strict exosomal hit and ranked fourth by perturbation impact, suggesting a broad indirect network role despite the absence of direct TLR–CLASH interactions (Fig. 4).

[Figure 4 here]

Figure 4. **Network perturbation ranking of exosomal EBV miRNAs.**

Alt text: Horizontal bar chart ranking exosomal EBV miRNAs by their impact on weighted TLR network reachability after in silico single-miRNA removal. BART17-5p shows the largest reduction in modelled TLR reachability at 37.3%, followed by BART8-3p at 21.7%, BART10-3p at 20.3%, and BART1-5p at 17.1%.

Table 5 lists the hub rankings. Sensitivity analysis using a STRING confidence threshold of 0.7 retained BART17-5p, BART8-3p, and BART10-3p among the highest-ranked exosome-associated miRNAs, supporting the robustness of the prioritisation. The three highest-ranked miRNAs were all Group B species with individual reachability reductions of 37.28% for BART17-5p, 21.72% for BART8-3p, and 20.27% for BART10-3p. As these values were computed from separate single-node perturbations, they were interpreted as individual prioritisation scores rather than as additive combined effects.

Table 5
EBV exosomal miRNA hub ranking by in silico knockdown impact

Rank	miRNA	Betweenness	Degree	Strength	Delta reachability	% Reduction	Group
1	ebv-miR-BART17-5p	0.834	3,279	26,164	4,354	37.28%	B
2	ebv-miR-BART8-3p	0.313	1,580	8,971	2,537	21.72%	B
3	ebv-miR-BART10-3p	0.246	1,088	7,695	2,367	20.27%	B
4	ebv-miR-BART1-5p	0.301	1,448	8,113	2,001	17.13%	A
5	ebv-miR-BART13-5p	0.068	421	1,584	317	2.72%	B
6	ebv-miR-BART2-3p	0.021	163	484	103	0.88%	A

Focused tripartite subnetworks were generated for the TLR7/8 ssRNA-sensing axis and TLR9/type I interferon axis. These sub-networks illustrate how exosomal EBV miRNAs connect to TLR modules through CLASH target genes and STRING PPI bridges. Given that both subnetworks are mechanistic visualisations rather than separate statistical results, they are provided in Supplementary Figures S7 and S8.

- SNU719 RNA-seq supports expression of most prioritised TLR-pathway targets

Of the 38 genes in the curated TLR pathway set, 36 were detected in the SNU719 RNA-seq after Ensembl-to-symbol mapping. IKBKE and IKBKG were not recovered in the mapped symbol space. Among the detected genes, 14 were highly expressed above 100 mean counts, 4 were expressed at 10–99 counts, 10 had low counts, and 8 were not detected above the background.

All seven CLASH-supported TLR pathway target genes with available RNA-seq data were expressed above the 10 CPM threshold: TAB2, NFKB1, NFKB2, RELA, IRAK1, IRF3, and TIRAP. TAB2 was the most highly expressed gene in the curated panel, followed by NFKB1, TBK1, NFKB2, MYD88, and RELA. These results indicate that the prioritised CLASH targets are not low-expression background genes; rather, they are transcriptionally detectable in SNU719 cells. Next, we evaluated whether the prioritised CLASH-supported targets were expressed in SNU719 cells, as miRNA target binding is biologically meaningful only when the target transcript is present (Fig. 5).

[Figure 5 here]

Figure 5. **Toll-like receptor (TLR)-pathway gene expression in SNU719 cells.**

Alt text: Horizontal bar chart showing mean expression of curated TLR-pathway genes in SNU719 cells using GSE239994 RNA-seq data. CLASH-validated EBV miRNA target genes are marked with asterisks. TAB2, NFKB1, NFKB2, RELA, IRAK1, IRF3, and TIRAP are transcriptionally detectable, supporting the biological plausibility of the prioritised miRNA-target interactions

Small RNA sequencing from the GSE147228 companion files was used to contextualise EBV latency and BART miRNA abundance. BART10-3p was the most abundant BART miRNA in this dataset, followed by BART6-3p and

BART8-5p. The BART:BHRF1 expression ratio was 1,192.9, supporting a BART-dominant latency-compatible profile. Latency and abundance analyses are shown in Supplementary Figure S9.

Directional miRNA-target concordance showed a negative regression slope across expression-filtered CLASH-supported pairs. However, this analysis used separate miRNA and mRNA datasets and had limited statistical power. Therefore, the directional miRNA-target concordance analysis is presented as a descriptive context only in Supplementary Figure S10.

Integrated evidence tiering distinguished expression-confirmed candidates from CLASH-supported interactions that lacked transcriptomic confirmation (Table 6). Three interactions reached tier 1 status: BART8-3p to NFKB1, BART17-5p to NFKB2, and BART17-5p to TAB2. Seven additional interactions reached Tier 2, including the convergent targeting of IRAK1, IRF3, TIRAP, RELA, and NFKB2. The binding of BART17-5p to IKBKG was retained in Tier 3 as IKBKG was not detected in the SNU719 RNA-seq symbol-mapped matrix. Thus, the expression-confirmed core consists of 10 miRNA-target pairs involving seven TLR/NF-κB/IRF pathway genes.

Table 6
Integrated evidence tiers for CLASH-supported EBV exosomal miRNA to TLR-pathway interactions.

miRNA	Target	CLASH score	Max score	Target expressed	Exo-enriched	Network hub	Literature context	Evidence score	Tier
ebv-miR-BART8-3p	NFKB1	10.53	26.31	Yes (high)	Yes (B)	Yes	Yes	5	Tier 1
ebv-miR-BART17-5p	NFKB2	9.57	25.07	Yes (high)	Yes (B)	Yes	No	4	Tier 1
ebv-miR-BART17-5p	Table 2	3.11	7.33	Yes (high)	Yes (B)	Yes	Yes	4	Tier 1
ebv-miR-BART8-3p	NFKB2	4.77	9.02	Yes (high)	Yes (B)	Yes	No	3	Tier 2
ebv-miR-BART17-5p	IRAK1	3.11	7.33	Yes (high)	Yes (B)	Yes	No	3	Tier 2
ebv-miR-BART10-3p	IRAK1	3.11	7.33	Yes (high)	Yes (B)	Yes	No	3	Tier 2
ebv-miR-BART10-3p	IRF3	1.55	2.65	Yes (expressed)	Yes (B)	Yes	No	3	Tier 2
ebv-miR-BART8-3p	IRF3	1.55	2.65	Yes (expressed)	Yes (B)	Yes	No	3	Tier 2
ebv-miR-BART17-5p	TIRAP	1.55	2.65	Yes (expressed)	Yes (B)	Yes	No	3	Tier 2
ebv-miR-BART17-5p	RELA	1.55	2.65	Yes (expressed)	Yes (B)	Yes	No	3	Tier 2
ebv-miR-BART17-5p	IKBKG	2.10	4.29	Not detected	Yes (B)	Yes	No	2	Tier 3

IKBKG was retained as CLASH-supported; however, it was not included in the expression-confirmed interaction set, as it was not detected in the SNU719 RNA-seq symbol-mapped matrix.

- TCGA-STAD bulk-tumour analysis does not show a strong EBV-dependent TLR pathway signature

GDC API mapping resolved the file UUIDs into 12-character TCGA patient barcodes. Cross-referencing with a curated EBV-positive barcode list identified 25 EBV-positive patients among the 439 subtype-mapped TCGA-STAD cases. Of these, 22 EBV-positive and 390 EBV-negative cases matched the RNA-Seq data and were used for pathway scoring. ssGSEA covered 37 of the 38 curated TLR pathway genes across 412 RNA-seq patients.

EBV-positive and EBV-negative tumours did not differ significantly regarding TLR signalling, TLR sensor, adaptor, NF-κB, interferon-response, or cytokine ssGSEA scores after FDR correction (Fig. 6). Although several module medians differed numerically, the effect sizes were small relative to within-group variability and should not be interpreted as evidence of a robust EBV-status-dependent bulk-tumour signature. These results indicated that the SNU719 exosome-associated BART miRNA to the TLR axis was not captured as a simple pathway-level difference in unselected bulk TCGA-STAD RNA-seq.

[Figure 6 here]

Figure 6. **The Cancer Genome Atlas (TCGA)-Stomach Adenocarcinoma (STAD) Toll-like receptor (TLR) pathway module scores by Epstein–Barr virus (EBV) status.**

Alt text: Boxplots comparing TCGA-STAD ssGSEA pathway module scores between EBV-negative and EBV-positive tumours. Six modules are shown: TLR signalling, TLR sensors, TLR adaptors, NF-κB, IFN response, and cytokines. All comparisons are labelled non-significant, indicating no strong EBV-status-dependent bulk-tumour TLR pathway signature in TCGA-STAD.

Table 7
TCGA-STAD ssGSEA TLR pathway module scores by EBV status.

Pathway module	Gene set size	EBV+ median (n = 22)	EBV- median (n = 390)	Direction	Wilcoxon p	FDR
TLR_signalling	37	0.0076	0.0161	Lower in EBV+	0.983	0.983
TLR_sensors	6	-0.2514	-0.2758	Higher in EBV+	0.475	0.983
TLR_adaptors	3	0.3172	0.3165	Slightly higher in EBV+	0.624	0.983
NF-κB	7	0.3012	0.3113	Lower in EBV+	0.830	0.983
IFN_response	11	0.2629	0.2408	Higher in EBV+	0.548	0.983
Cytokines	8	-0.1604	-0.1904	Higher in EBV+	0.983	0.983

Since all FDR values were non-significant, Table 7 was interpreted as a negative contextual analysis rather than clinical validation of the SNU719-derived mechanism. A heatmap of the curated TLR genes confirmed broad pathway expression across TCGA-STAD; however, it did not show clear EBV-specific clustering, as shown in Supplementary Figure S11.

MCP-counter deconvolution was used to explore whether EBV-positive tumours showed differences in immune or stromal cell estimates. No cell type remained significant after FDR correction. The myeloid dendritic, monocyte/macrophage, endothelial, and fibroblast-associated scores showed numerical differences in some comparisons; however, these trends were not statistically significant. Therefore, immune deconvolution was treated

as an exploratory bulk tumour context rather than as a validation of the exosomal miRNA mechanism (Supplementary Figure S12).

Among the 22 EBV-positive TCGA-STAD tumours, Spearman's correlation analysis revealed the expected co-expression structure among several NF-κB, kinase, and interferon-response genes. However, given the small EBV-positive subset and the absence of patient-level EBV BART miRNA measurements, this analysis was interpreted as an exploratory pathway. A correlation heatmap is shown in Supplementary Figure S13.

Survival analyses did not support the prognostic effects of EBV status or TLR pathway scoring in the TCGA-STAD cohort. The Kaplan–Meier curves for EBV-positive versus EBV-negative tumours showed overlapping survival trajectories with log-rank p = 0.89. The median split TLR pathway score did not stratify survival (log-rank P = 0.48). In a Cox model including the TLR signalling score, IFN response score, EBV status, and AJCC pathological stage, stage was the only significant predictor of overall survival. These results are consistent with the interpretation that bulk tumour TLR pathway scores do not provide independent prognostic information in this cohort. Kaplan–Meier plots are provided in Supplementary Figures S14 and S15, and the Cox model is provided in Supplementary Figure S16.

The ACRG cohort was used only as an independent expression-context dataset as EBV status-specific comparisons were not available in the same form as TCGA-STAD. All the curated TLR pathway genes were detected on the microarray platform, confirming that the selected gene sets could be evaluated across independent gastric cancer transcriptomic datasets. Given the difference in ssGSEA score scales between the RNA-seq and microarray platforms, the absolute scores were not directly compared between TCGA-STAD and ACRG. These data support the portability of the scoring workflow; however, they do not constitute an independent validation of EBV-specific pathway modulation.

Discussion

- Coordinated multi-node targeting of TLR/NF-κB/IRF signalling by exosomal EBV BART miRNAs

Three exosome-associated EBV BART miRNAs show reproducible CLASH-supported binding to multiple components of the TLR/NF-κB/IRF signalling axis in SNU719 cells. BART8-3p and BART17-5p target NFKB1 and NFKB2, BART17-5p and BART10-3p converge on IRAK1, and BART8-3p and BART10-3p target IRF3. This arrangement is biologically meaningful, as these genes occupy different levels of innate immune signalling, including signal relay, NF-κB transcriptional output, and interferon regulatory control. The CLASH evidence demonstrates miRNA target binding and not repression by itself. Therefore, we interpreted these results as a prioritised map of candidate regulatory interactions that can be tested in recipient immune cells exposed to SNU719-derived exosomes.

This candidate regulatory architecture is consistent with the principle that EBV miRNAs reshape host immune signalling and immune escape programs [7]. Our results place exosome-associated EBV BART miRNAs within this context and identify specific SNU719-derived candidates that may influence innate immune signalling in EBVaGC.

- BART17-5p as a dominant candidate hub

Network topology analysis identified BART17-5p as the most influential exosome-associated EBV miRNA in the modelled TLR network. The betweenness centrality of BART17-5p was 0.834, higher than that of other exosomal miRNAs, and individual in silico removal of BART17-5p produced a 37.28% reduction in modelled TLR reachability.

BART17-5p also had the broadest direct CLASH-supported TLR pathway-targeting profile, engaging NFKB2, TAB2, IRAK1, IKBKG, TIRAP, and RELA. This combination of direct target breadth, centrality, and perturbation impact makes BART17-5p the clearest candidate for experimental prioritisation.

Among the evidence-tiered targets, BART17-5p bound to NFKB2 and BART17-5p bound to TAB2 were particularly strong candidates for reporter assays. The binding of BART8-3p to NFKB1 is also important, given its highest mean CLASH score in the expression-confirmed set. Future experimental studies should consider multi-miRNA perturbations since exosomes carry several BART species simultaneously. Such experiments would determine whether BART17-5p, BART8-3p, and BART10-3p act independently, additively, or synergistically on NF-κB and IRF outputs.

- BART1-5p and the distinction between abundance and pathway specificity

BART1-5p was the most abundant strictly enriched exosomal EBV miRNA, reaching 565,691 CPM in SNU719 exosomes and showing 3.43-fold enrichment over cells. However, BART1-5p had no direct reproducible CLASH interaction with the curated TLR pathway genes. This illustrates the important distinction between cargo abundance and pathway specificity. BART1-5p may have a broader role in exosomal biology or indirect pathway regulation than in direct TLR pathway targeting. Its fourth-place network perturbation ranking suggests that indirect connectivity through broad host targets may influence TLR-associated network reachability.

This pattern supports a possible division of labour within the exosomal EBV miRNA cargo. Highly abundant miRNAs, such as BART1-5p, may affect broad cellular processes, whereas less abundant and more pathway-focused miRNAs, such as BART17-5p, BART8-3p, and BART10-3p, may engage immune signalling nodes directly. This hypothesis should be tested experimentally rather than inferred solely from the network topology.

- TCGA-STAD contextualisation and limits of bulk-tumour validation

TCGA-STAD analysis provides useful boundary conditions for interpretation. Although EBV-positive cases were successfully mapped and pathway scores were computed across 412 tumours, EBV status was not associated with significant differences in bulk TLR, NF-κB, IFN-response, or cytokine ssGSEA scores. Survival analysis did not support an association between EBV status or TLR score and OS after accounting for stage. These negative findings should not be treated as failures of the computational framework. Rather, they highlighted an important biological and technical distinction: the proposed mechanism involves exosome-mediated communication between tumour and recipient immune cells, whereas TCGA-STAD measures bulk tumour RNA from mixed tumour, immune, and stromal compartments. Therefore, local vesicle-mediated regulatory effects may be diluted or masked in the bulk transcriptomes.

The TCGA results also clarified what this study can and cannot claim. The patient-cohort analysis shows that TLR/NF-κB/IRF pathway genes are broadly detectable in gastric tumours and that the analysis pipeline can be transferred to clinical transcriptomic data. This does not demonstrate that EBV-positive tumours have a robust bulk-TLR-suppressed phenotype. Future patient-level validation will require EBV miRNA-aware quantification from primary tumours, single-cell or spatial transcriptomics to resolve recipient immune compartments, and paired tumour-exosome profiling.

- Strengths and limitations

The primary methodological strength of this study was the use of the CLASH as the central interaction evidence source. Unlike prediction-only approaches such as TargetScan or miRDB, CLASH captures experimentally observed ago-associated miRNA-target binding in living cells [7]. All 11 reported TLR pathway interactions were present in all three SNU719 CLASH replicates. Integrating exosomal enrichment, CLASH evidence, STRING network topology, and SNU719 RNA-seq expression filtering provided a stronger prioritisation framework than any single evidence layer alone.

This study has several limitations. First, the exosomal enrichment analysis used three biological replicates per group. Although this is common in public small-RNA datasets, it limits the power to detect modest enrichment. For this reason, BART17-5p, BART10-3p, and BART8-3p were considered moderately enriched candidates rather than strict FDR-significant exosomal hits. Second, CLASH identifies Ago-associated miRNA-target binding; however, it does not prove target repression or pathway inhibition. Third, the miRNA-target concordance analysis used separate small RNA and mRNA datasets; therefore, it was interpreted only as a directional context. Fourth, no new exosome characterisation was performed, and the EV identity of the source samples was based on the original GSE227017 study [8]. Fifth, TCGA-STAD bulk RNA-seq cannot distinguish tumour cell TLR expression from immune or stromal expression and cannot directly measure exosome-recipient-cell communication. Sixth, the GDC-processed miRNA files did not include EBV BART miRNA quantification, preventing patient-level correlations between BART miRNA abundance and TLR pathway activity.

- Future experimental directions

The computational predictions suggest several specific experimental directions. First, dual-luciferase reporter assays should test BART8-3p for NFKB1, BART17-5p for NFKB2, BART17-5p for TAB2, and BART10-3p for IRAK1 or IRF3. Second, SNU719-derived exosomes should be transferred to macrophages or dendritic cells followed by TLR7/8 or TLR9 agonist challenge to measure NF-κB nuclear translocation, IRF3 activation, and cytokine release. Third, BART miRNA inhibitors or engineered exosome models can be used to assess whether the candidate miRNAs act independently or cooperatively. Finally, patient-level validation would benefit from single-cell, spatial, or exosome-enriched profiling of EBV-positive gastric tumours.

Conclusions

This study presents an integrative computational framework linking SNU719 exosome-associated EBV BART miRNA enrichment, SNU719-specific CLASH interactions, network topology, transcriptomic target filtering, and TCGA-STAD bulk tumour contextualisation. The core finding is that three moderately exosome-enriched EBV BART miRNAs, BART17-5p, BART8-3p, and BART10-3p, show reproducible CLASH-supported binding to TLR/NF-κB/IRF pathway components, including NFKB1, NFKB2, TAB2, IRAK1, IRF3, TIRAP, and RELA. Network perturbation prioritised BART17-5p as the dominant candidate hub, whereas SNU719 RNA-seq confirmed the expression of 10 miRNA-target pairs involving seven pathway genes.

TCGA-STAD analysis did not identify significant EBV status-dependent differences in bulk TLR, NF-κB, interferon-response, or cytokine pathway scores, nor did EBV status or TLR score significantly stratify survival. These findings indicate that the proposed SNU719 exosome-associated BART miRNA axis is best interpreted as a candidate local cell–cell communication mechanism, rather than a robust bulk-tumour transcriptional signature. The prioritised interactions, especially BART8-3p to NFKB1, BART17-5p to NFKB2, BART17-5p to TAB2, and BART10-3p to IRAK1 or IRF3, provided specific testable hypotheses for reporter assays, miRNA perturbations, and exosome-recipient-cell immune challenge models.

Declarations

Ethics approval and consent to participate

Not applicable

Consent for publication

Not applicable

Funding

This research was supported by the Regional Innovation System & Education (RISE) program through the Gwangju RISE Center, funded by the Ministry of Education (MOE) and the Gwangju Metropolitan City, Republic of Korea (2026-RISE-05-013).

Author Contribution

M.C. contributed to design of the work, analysis, interpretation of data, preparing figures and writing the main manuscript text. S.R.H. contributed to conception, project administration, supervision, and writing and revising the manuscript. All authors reviewed the manuscript.

Acknowledgement

The authors gratefully acknowledge the research groups that generated and publicly deposited these datasets used in this study. The authors gratefully acknowledge the research groups that generated and publicly deposited the datasets used in this study. The authors acknowledge Lin et al. for generating and depositing the SNU719 exosomal miRNA-seq data under GEO accession GSE227017. The authors acknowledge Ungerleider et al. for generating and depositing the EBV miRNA CLASH interaction data under GEO accession GSE147228. The authors acknowledge Maestri et al. for generating and depositing the SNU719 whole-transcriptome RNA-seq data under GEO accession GSE239994. The authors acknowledge Cristescu et al. for generating and depositing the ACRG gastric cancer cohort microarray data under GEO accession GSE62254.The results shown here are, in whole or in part, based on data generated by the TCGA Research Network: https://www.cancer.gov/tcga. TCGA-STAD data were generated with support from the National Cancer Institute and National Human Genome Research Institute. The authors thank the NCI Genomic Data Commons for maintaining the open-access data infrastructure and the NCBI GEO team for hosting the public sequencing datasets that made this computational study possible.

Data Availability

All datasets analysed in this study are publicly available from established genomic repositories and no new datasets were generated. The SNU719 exosome miRNA-seq data (GSE227017), CLASH interaction data (GSE147228), SNU719 whole transcriptome RNA-seq data (GSE239994), and ACRG gastric cancer expression-context microarray data (GSE62254) are all available from NCBI GEO at https://www.ncbi.nlm.nih.gov/geo/. The TCGA-STAD open-access miRNA-seq, RNA-seq, and clinical data are available from the NCI Genomic Data

Commons at https://portal.gdc.cancer.gov/. The protein-protein interaction data used for network construction are available from the STRING database at https://string-db.org/. Project name: EBVaGC exosomal BART miRNA CLASH-network analysis.Project home page: https://github.com/MeghaChandran06/ebvagc-exosomal-bart-tlr-network Operating system: Platform independent.Programming language: R.Other requirements: R package versions are provided in the repository.Restrictions to be used by non-academics: None.

References

1. Morgan E, et al. The current and future incidence and mortality of gastric cancer in 185 countries, 2020–40: A population-based modelling study. eClinicalMedicine. 2022;47:101404.
2. The Cancer Genome Atlas Research Network. Comprehensive molecular characterization of gastric adenocarcinoma. Nature. 2014;513:202–9.
3. Théry C, Witwer KW, Aikawa E, et al. Minimal information for studies of extracellular vesicles 2018 (MISEV2018): a position statement of the International Society for Extracellular Vesicles and update of the MISEV2014 guidelines. J Extracell Vesicles. 2018;7(1):1535750.
4. Kalluri R, LeBleu VS. The biology, function, and biomedical applications of exosomes. Science. 2020;367(6478):eaau6977.
5. Pegtel DM, Cosmopoulos K, Thorley-Lawson DA et al. Functional delivery of viral miRNAs via exosomes. *Proceedings of the National Academy of Sciences USA* 2010;107(14):6328–33.
6. Meckes DG, Shair KHY, Marquitz AR, et al. Human tumor virus utilizes exosomes for intercellular communication. Proc Natl Acad Sci U S A. 2010;107(47):20370–5.
7. Ungerleider N, Bullard W, Kara M, et al. EBV miRNAs are potent effectors of tumor cell transcriptome remodeling in promoting immune escape. PLoS Pathog. 2021;17(5):e1009217. https://doi.org/10.1371/journal.ppat.1009217.
8. Lin M, Hu S, Zhang T, et al. Effects of co-culture EBV-miR-BART1-3p on proliferation and invasion of gastric cancer cells based on exosomes. Cancers. 2023;15(10):2841.
9. Kawai T, Akira S. Toll-like receptors and their crosstalk with other innate receptors in infection and immunity. Immunity. 2011;34(5):637–50.
10. Lind NA, Rael VE, Pestal K, et al. Regulation of the nucleic acid-sensing Toll-like receptors. Nat Rev Immunol. 2022;22(4):224–35.
11. Ungerleider N, Bullard W, Kara M, et al. EBV miRNAs are potent effectors of tumor cell transcriptome remodeling in promoting immune escape. PLoS Pathog. 2021;17(5):e1009217.
12. The Cancer Genome Atlas Research Network. Comprehensive molecular characterization of gastric adenocarcinoma. Nature. 2014;513:202–9.
13. Maestri D, Napoletani G, Kossenkov A, et al. The three-dimensional structure of the EBV genome plays a crucial role in regulating viral gene expression in EBVaGC. Nucleic Acids Res. 2023;51(22):12092–110.
14. Cristescu R, Lee J, Nebozhyn M, et al. Molecular analysis of gastric cancer identifies subtypes associated with distinct clinical outcomes. Nat Med. 2015;21(5):449–56.
15. Robinson MD, McCarthy DJ, Smyth GK. edgeR: a Bioconductor package for differential expression analysis of digital gene expression data. Bioinformatics. 2010;26(1):139–40.
16. Yu G, Wang LG, Han Y, et al. clusterProfiler: an R package for comparing biological themes among gene clusters. OMICS. 2012;16(5):284–7.

17. Csárdi G, Nepusz T. The igraph software package for complex network research. InterJournal Complex Syst 2006;1695.
18. Pedersen TL. ggraph: An Implementation of Grammar of Graphics for Graphs and Networks. 2022.
19. Hänzelmann S, Castelo R, Guinney J. GSVA: gene set variation analysis for microarrays and RNA-seq data. BMC Bioinformatics. 2013;14:7.
20. Sturm G, Finotello F, Petitprez F, et al. Comprehensive evaluation of transcriptome-based cell-type quantification methods for immunooncology. Bioinformatics. 2019;35(14):i436–45.
21. Therneau TM. A Package for Survival Analysis in R, version 3.8-6. 2026.

Figures

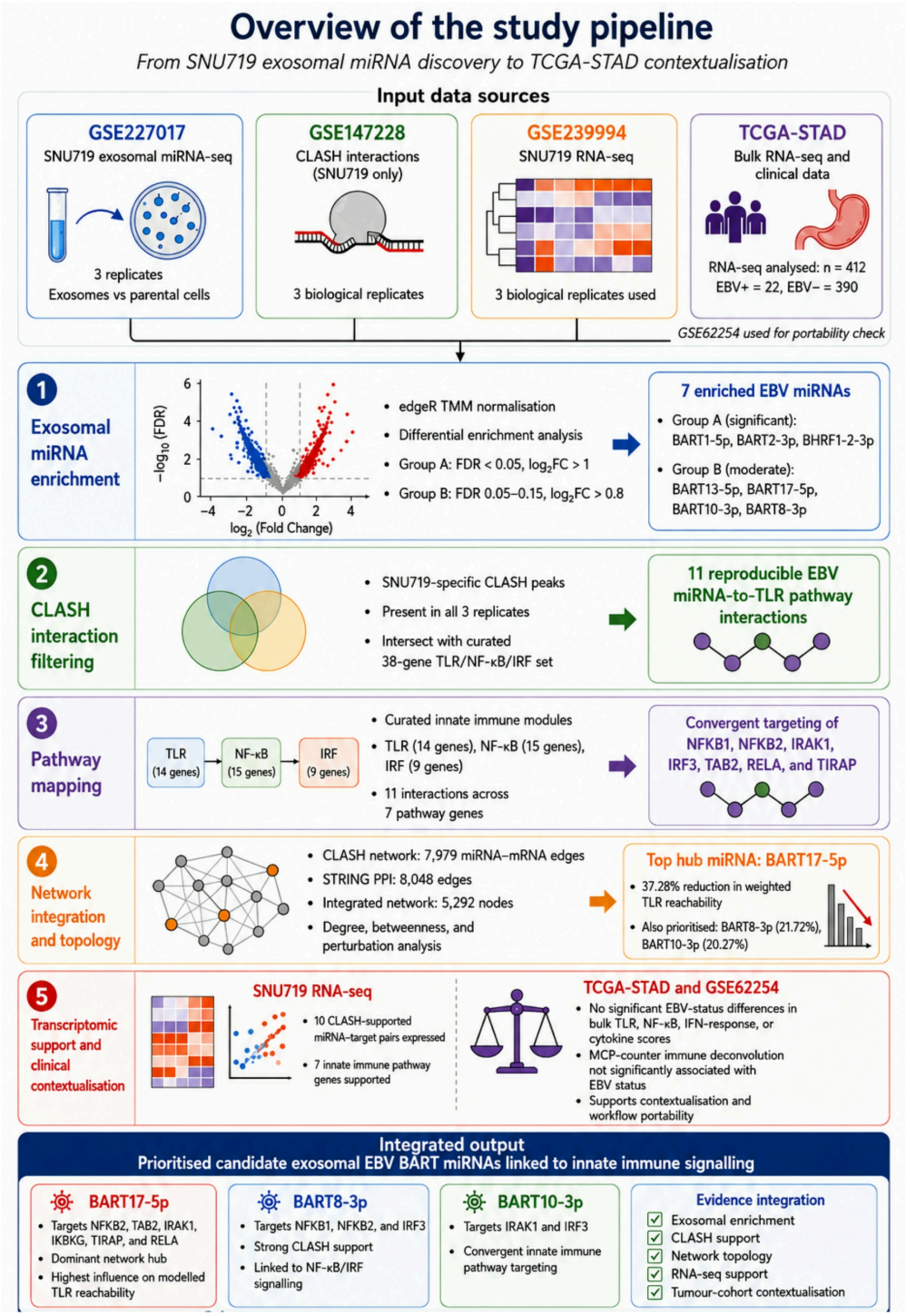


Figure 1

Overview of the CLASH-guided multilayer evidence framework used to prioritise exosomal EBV BART miRNA-host interactions in EBV-associated gastric cancer.

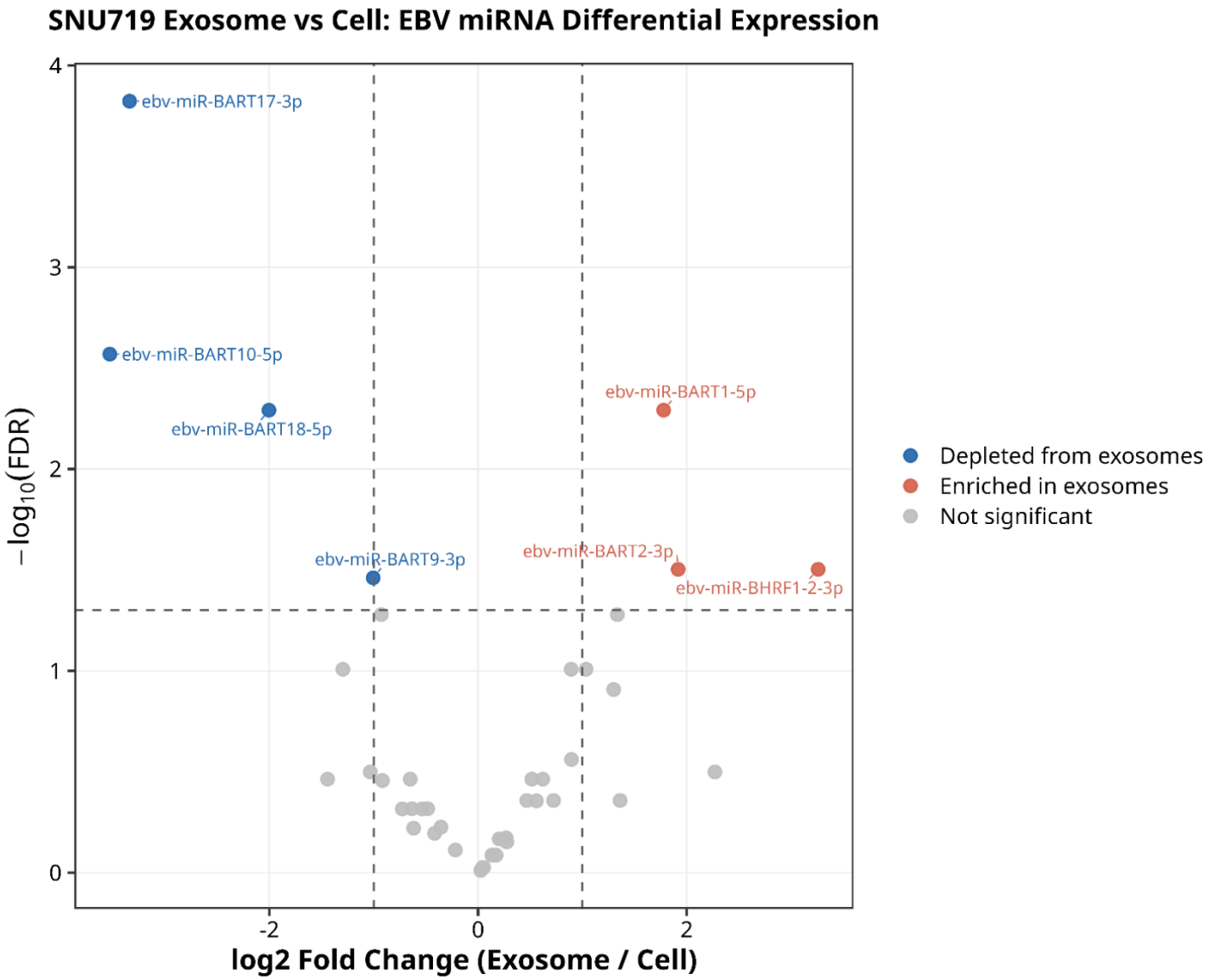


Figure 2

Differential EBV miRNA enrichment in SNU719 exosomes.

Alt text: Volcano plot comparing EBV miRNA enrichment between SNU719 exosomes and SNU719 cells. Red points indicate miRNAs enriched in exosomes, blue points indicate miRNAs depleted from exosomes, and grey points indicate non-significant miRNAs. BART1-5p, BART2-3p, and BHRF1-2-3p are enriched in exosomes, while BART17-3p and other miRNAs are depleted.

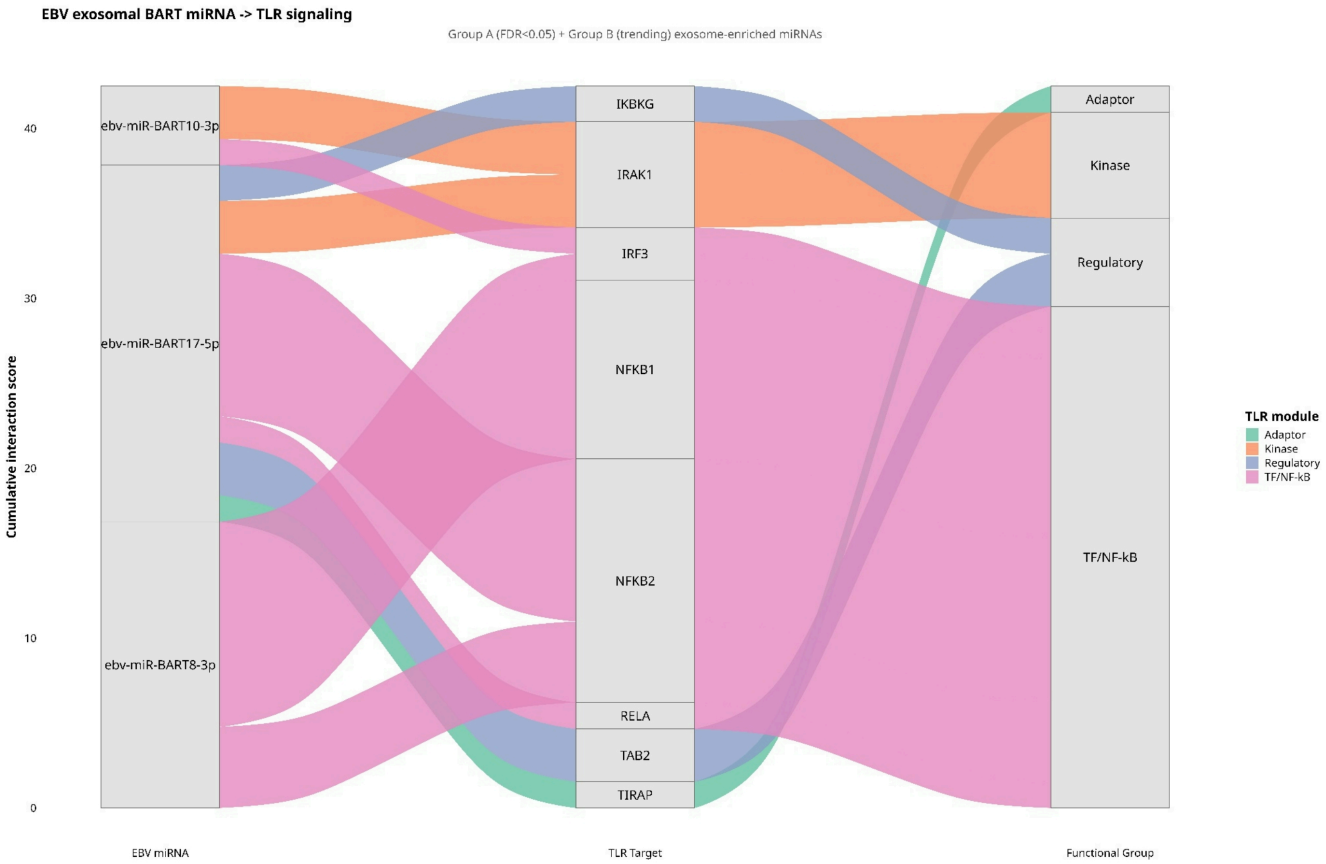


Figure 3

Reproducible Epstein–Barr virus (EBV) microRNA (miRNA) interactions using Toll-like receptor (TLR)-pathway genes.

Alt text: Alluvial plot showing reproducible EBV miRNA interactions with TLR pathway genes based on SNU719 CLASH data. BART17-5p, BART8-3p, and BART10-3p connect to TLR-related targets including NFKB1, NFKB2, IRAK1, IRF3, TAB2, TIRAP, RELA, and IKBKG, with flows grouped into adaptor, kinase, regulatory, and TF/NF-κB functional modules.

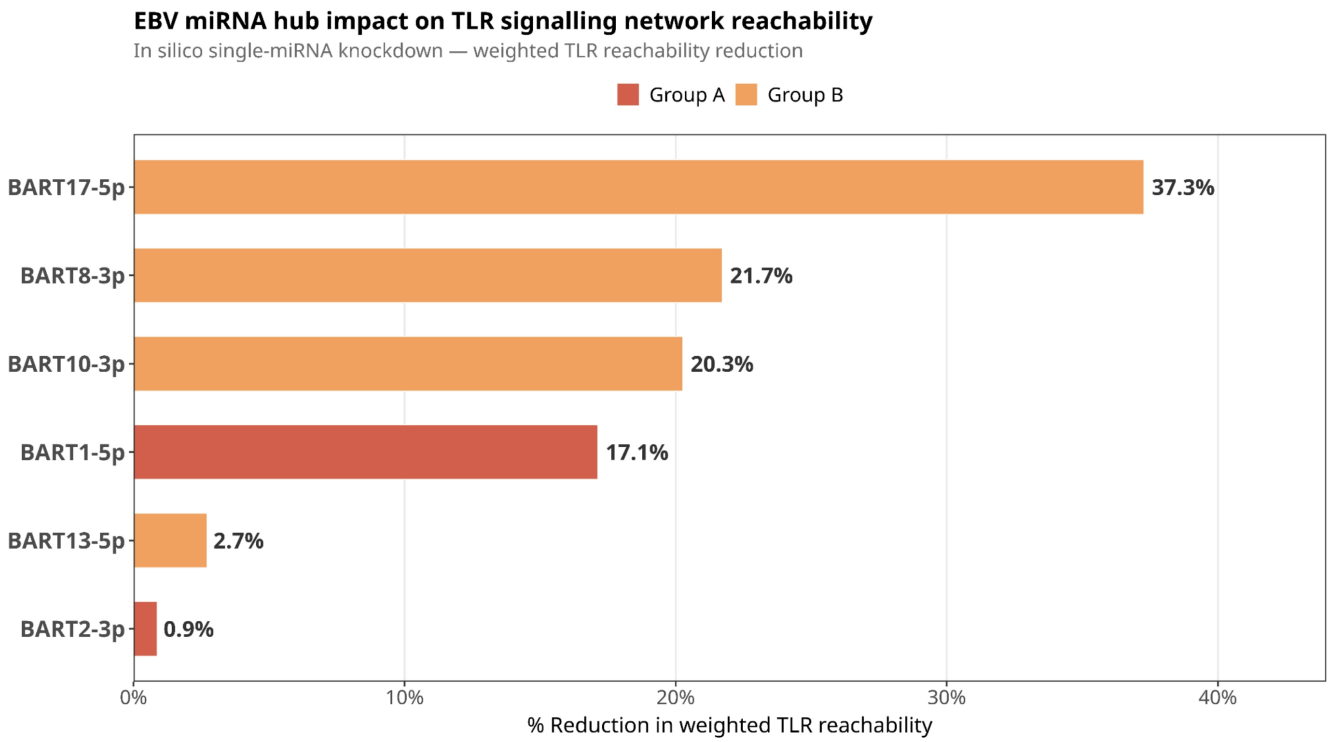


Figure 4

Network perturbation ranking of exosomal EBV miRNAs.

Alt text: Horizontal bar chart ranking exosomal EBV miRNAs by their impact on weighted TLR network reachability after in silico single-miRNA removal. BART17-5p shows the largest reduction in modelled TLR reachability at 37.3%, followed by BART8-3p at 21.7%, BART10-3p at 20.3%, and BART1-5p at 17.1%.

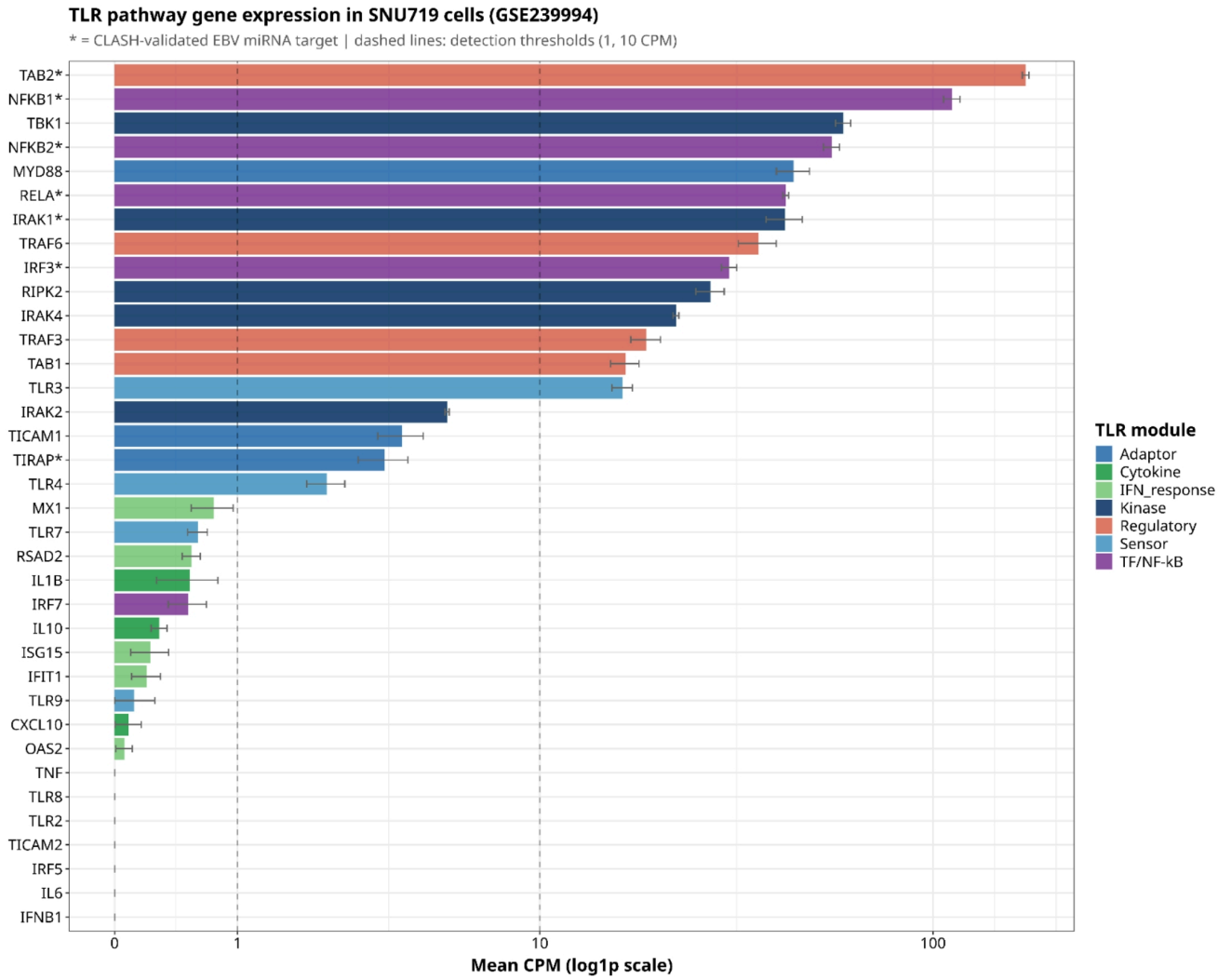


Figure 5

Toll-like receptor (TLR)-pathway gene expression in SNU719 cells.

Alt text: Horizontal bar chart showing mean expression of curated TLR-pathway genes in SNU719 cells using GSE239994 RNA-seq data. CLASH-validated EBV miRNA target genes are marked with asterisks. TAB2, NFKB1, NFKB2, RELA, IRAK1, IRF3, and TIRAP are transcriptionally detectable, supporting the biological plausibility of the prioritised miRNA-target interactions

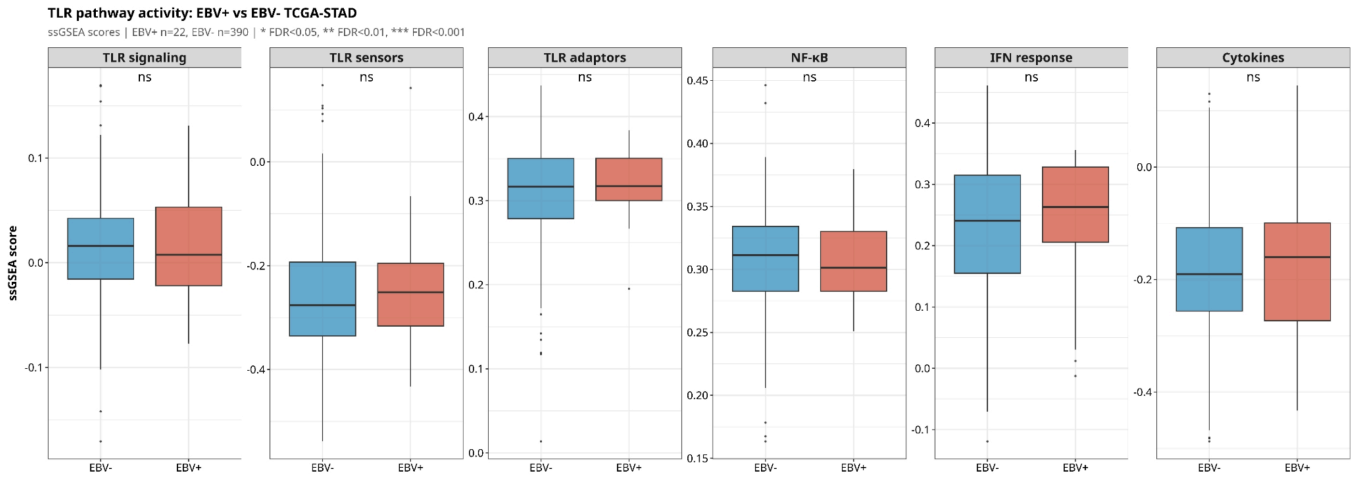


Figure 6

The Cancer Genome Atlas (TCGA)-Stomach Adenocarcinoma (STAD) Toll-like receptor (TLR) pathway module scores by Epstein–Barr virus (EBV) status.

Alt text: Boxplots comparing TCGA-STAD ssGSEA pathway module scores between EBV-negative and EBV-positive tumours. Six modules are shown: TLR signalling, TLR sensors, TLR adaptors, NF-κB, IFN response, and cytokines. All comparisons are labelled non-significant, indicating no strong EBV-status-dependent bulk-tumour TLR pathway signature in TCGA-STAD.

Supplementary Files

This is a list of supplementary files associated with this preprint. Click to download.

- Additionalfile1Supplementaryfigures.zip
- Additionalfile2Supplementarytables.docx